FULL PAPER

Top-Down Fabrication of High Quality III–V Nanostructures by Monolayer Controlled Sculpting and Simultaneous Passivation

*Shagufta Naureen, Naeem Shahid, Reza Sanatinia, and Srinivasan Anand**

In the fabrication of III–V semiconductor nanostructures for electronic and optoelectronic devices, techniques that are capable of removing material with monolayer precision are as important as material growth to achieve best device performances. A robust chemical treatment is demonstrated using sulfur (S)-oleylamine (OA) solution, which etches layer by layer in an inverse epitaxial fashion and simultaneously passivates the surface. The application of this process to push the limits of top-down nanofabrication is demonstrated by the realization of InP-based high optical quality nanowire arrays, with aspect ratios more than 50, and nanostructures with new topologies. The findings are relevant for other III–V semiconductors and have potential applications in III–V device technologies.

1. Introduction

III–V semiconductor nanostructures have attracted tremendous attention for their unique physical properties, and for potential applications in electronics and optoelectronics,[1–5] thermoelectrics,[6] sensing, and biological sciences.[7,8] Simplicity, low cost, and precision in fabrication are some of the important factors in the processing of semiconductor nanostructures and devices. At each process step, nanometer or sub-nanometer scale fabrication precision and control is necessary for several nanodevices/structures. III–V semiconductors are widely used for a variety of electronic and optoelectronic devices. Hence, there is substantial research effort on these materials and device technologies to improve device performance and/or to provide new functionality by utilizing nanostructures. In addition, as projected by the International Technology Roadmap for Semiconductors (ITRS 2011) III–V materials are attractive for emerging and future technology. For example, III–V materials are attractive candidates for the high mobility channel layers in future high speed and low-power electronic components.[9]

Metal organic vapor phase epitaxy (MOVPE) and molecular beam epitaxy (MBE) are epitaxial growth techniques that have atomic layer precision for growth of III–V layers. Precise control over layer thickness, material mole fraction and dopant concentration is a key factor for devices such as high electron mobility transistors (HEMTs),[10] nanowire field effect transistors (NWSFETs),[11] quantum well or quantum dot lasers.[12,13] Top-down processing steps, e.g. patterning and dry etching, are very common in the fabrication of these devices. However, surface damage during fabrication and limitations on fabrication accuracy affect device performance adversely. In both top-down and bottom-up fabrication of III–V semiconductor nanopillar/nanowire devices, significant effort is required to control nanowire morphology and size. In addition, non-radiative surface recombination has to be minimized, and new methods for surface passivation are continually being developed.[14,15] As with electronic devices, the physical size, material properties, fabrication precision, and the quality of the structures are also deciding factors in many photonic devices. For example, sub-nanometer deviation in hole size and/or position are known to affect the resonance position of photonic crystal cavities,[16] and precise modification of the fabricated structure to tune cavity resonance(s) is often necessary.[17]

Techniques capable of removing material with monolayer precision are as important as material growth to realize best device performances. Such techniques can be employed in a novel way for controlled sculpting of fabricated (top-down or bottom-up) nanostructures to obtain new shapes and topologies of nanostructures. In addition, physical dimensions of structures can be reduced beyond what is possible with a given fabrication technique. For example, using top down approaches, fabrication of structures with lateral dimensions of one to few tens of nanometers requires high resolution lithography and highly resistant masks. Lastly, the surface damage induced by dry etching will have a dominant influence on their electrical and optical properties. Conventional photolithography in combination with dilute wet chemical etching has been used to fabricate InP and GaAs nanowires.[18] However, the side-walls were reported to be rough, which could adversely affect their electrical and optical properties.[18] In general, with conventional wet and dry etching methods it is very difficult to achieve atomic layer control. A two-step chemical etching technique, called digital etching, has been used for nanoscale etching. This technique typically involves self-limiting oxidation of the material and subsequent removal of the formed oxide layer,[19,20] and

S. Naureen, N. Shahid, R. Sanatinia, Dr. S. Anand
School of Information and Communication Technology
KTH-Royal Institute of Technology
Electrum 229, Kista S-14164 Sweden
E-mail: anand@kth.se

DOI: 10.1002/adfm.201202201

have been developed for GaAs,[20] Si,[21] and InP.[22] By sequential repetition of the oxidation and oxide-removal cycle, the material can be removed in a controlled way. However, this approach is cumbersome if several layers of the material have to be removed. Etching with monolayer control diamond[23] and InP[24] using hydrogen plasma and Ne ion irradiation, respectively, has been reported. Mostly, such processes have low throughput, high cost and can cause surface damage due to ion bombardment. Surface passivation is critical for several devices, irrespective of the method, and is often a separate process step. Thus, it would be a distinct advantage if the same process used for high precision etching can simultaneously provide effective surface passivation.

Here, we report, for first time, a novel single step chemical etching process based on dissolving sulfur in oleylamine (OA). The process is applicable for several III–V materials, provides highly controlled etch-rates, and simultaneously passivates the surface. The applications of this process are primarily demonstrated in the InP-based materials; although, other materials such as GaAs, InAs, InSb, and GaP are also investigated. A striking illustration is the etching of an epitaxial (100) InP wafer, wherein the monolayer (ML) steps are still retained even after removing 50 nm of the material. Using this process, we demonstrate high precision sculpting of InP-based nanostructures to obtain high optical quality nanomesh structures and high aspect ratio nanopillars. In addition, we show that the simultaneous surface passivation obtained with the etch process provides significant enhancement in the photoluminescence intensities of InP and GaAs. The findings are potentially interesting for III–V nanostructures and associated devices, gate recess etching of III–V based electronic devices such as HEMTs, fine tuning of resonant optical structures, and generation of new nanostructure topologies.

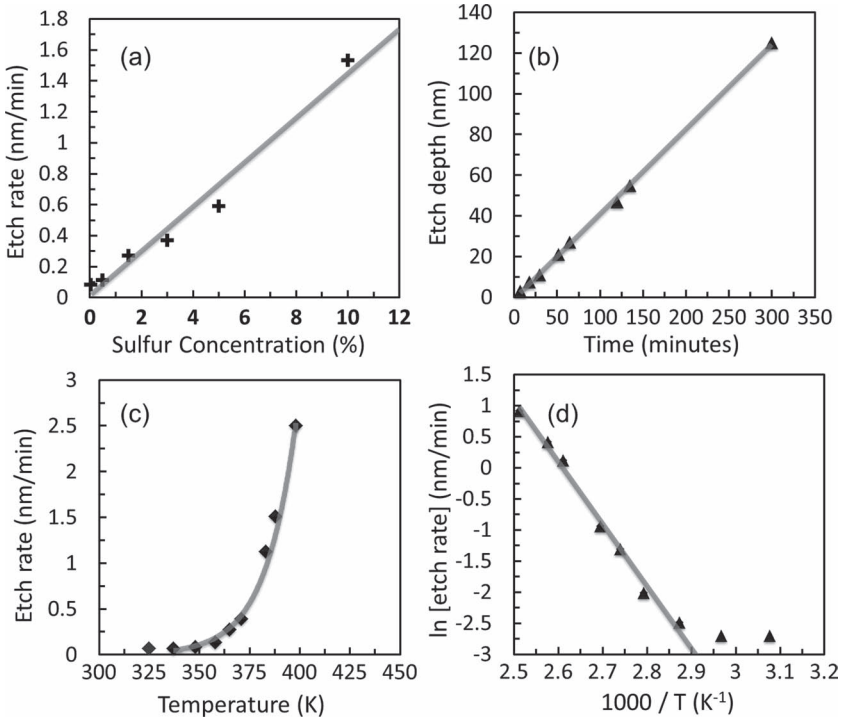

Figure 1. Etching of InP in S-OA solution: a) dependence of etch-rate on sulfur concentration. 2 h etching at 95 °C for all samples. b) Etch depth as a function of etch time at constant temperature and concentration. c) Etch rate vs. temperature and d) the corresponding Arrhenius plot. The activation energy calculated from the slope of the fitted line is 83 meV.

2. Results and Discussion

We have used a chemical solution prepared by dissolution of sulfur in OA, a primary amine, for etching as well as for passivation. Hereafter, we will refer to this solution as S—OA solution. Organic polysulfides (as a reaction of S and OA) formed in the solution with an amine chain could bind to the surface forming a film. Consequently, etching can occur in an inverse epitaxial manner, and sulfur could act to passivate the surface. Primary amines (R-NH_2) have been used to form self-assembled monolayers (SAMs) on metals and semiconductors.[25] Passivation using ammonium and sodium sulphides,[26] and SAMs of alkanthiols[27–30] have been extensively investigated for passivation of III–V semiconductors such as InP and GaAs. Recently, other approaches derived from solution chemistry used for quantum dot synthesis have also been used.[31,32]

Figure 1 shows the measured etch characteristics of the S—OA solution (depth and rate) for InP as a function of different etch-parameters. As shown in Figure 1a, the etch rate increases linearly with sulfur concentration in the S—OA solution. This clearly indicates that the chemical products resulting from the reaction between sulfur and oleylamine are responsible for etching. A linear relation of the etch depth with etch (treatment) duration is observed, as shown in Figure 1b, confirming that the process is rate limited. The etch depth can be varied from very low (few nanometers) to over 100 nm by varying the etch duration, using a 1.5% sulfur solution at a fixed temperature. The surface morphology, as measured by atomic force microscopy (AFM), remains very smooth, even after 5 h of etching time, with rms. roughness comparable to the untreated surface. The temperature dependence of the etch rate is investigated using 1.5% sulfur solution, keeping the etch time fixed (2 h). For these experiments separate solutions were prepared at 70–75 °C. For treatment at lower temperatures, the solution is cooled to the designated temperature and maintained at that temperature for 2 h. As shown in Figure 1c, the etch rate is thermally activated, typical for rate-limiting processes, and varies exponentially with temperature. The corresponding Arrhenius plot is shown on Figure 1d, and the determined activation energy E_a for the reaction is 83 meV. To verify the applicability of this etch-process for other binary III–V semiconductors, preliminary experiments on GaP, GaAs, InAs, and InSb were made at 94 °C using a 1.5% sulfur solution. The results are shown in the Supporting Information (Figure S1). Etch rate for InSb was highest, ≈3 nm/min, while for GaP it was

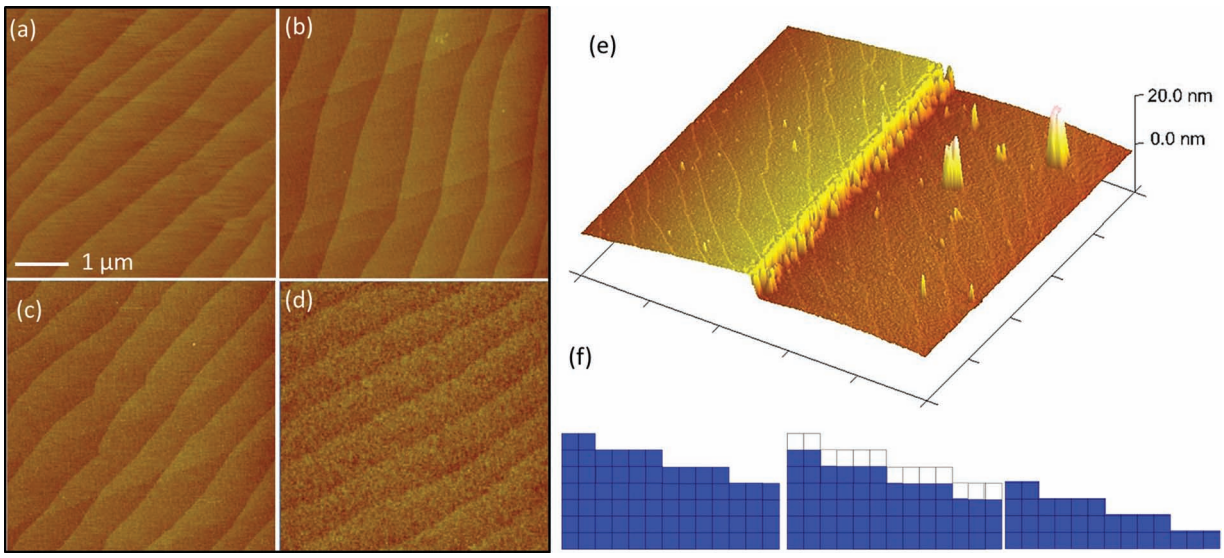

Figure 2. AFM images showing the surface morphology of (100) InP (epitaxial) samples (scan size: 5 × 5 μm^2): a) as-grown epitaxial surface, b) after etching 2 nm (5 min), c) after 11 nm etching (30 min), and d) after etching 55 nm (135 min). e) AFM topography on a 5 × 5 μm^2 area of a patterned epitaxial InP sample showing the steps and its continuity on the etched and unetched regions. The irregularities/roughness at the border between the etched and unetched regions is due to irregularities in the mask-definition processes. f) Schematic illustration of the step by step etching which maintains the epitaxial step flow morphology: i) surface with step flow before etching and ii,iii) after etching one and three monolayers, respectively.

0.03 nm/min; intermediate values were obtained for InAs (1.8 nm/min), InP (0.4 nm/min) and GaAs (0.1 nm/min). These results show the expected trend with the bond strengths of the materials. A detailed investigation is necessary for a comprehensive analysis of etching of these materials, and is beyond the scope of the present work.

The morphologies of the etched InP surfaces were also investigated by AFM. Although, higher etch rates could be obtained at higher S-concentration and/or temperature, in terms of surface morphology the best results were obtained with 1.5% S solution at 90–100 °C. Under these conditions, etch-rates were in the range of 0.25–0.5 nm/min. Remarkably, the epitaxially grown InP surfaces maintain their step-flow morphology as the samples are progressively etched. This is clearly visible on the representative AFM images of the as-grown and the etched sample surfaces displayed on **Figure 2**a–d. These results illustrate a novel atomic layer etching process, wherein the step flow morphology could be observed for as much as ≈55 nm of etching. AFM topography (representative) of a patterned epitaxial sample also shows the ML steps on the un-etched and the etched regions (Figure 2e). The ML steps appear continuous, which strongly indicates that the etching occurs predominantly from the top surface and the etch-front propagates without degradation of the atomic layer steps. The results were similar in other regions of the sample, and in larger scanned areas (≈100 μm^2). The above observations suggest the formation of a highly uniform etchant layer, similar to SAM, on the surface. A schematic illustration for this monolayer by monolayer etching process is shown on Figure 2f. Here, we comment that the apparent difference in the step directions between AFM images (Figure 2a–d) is due to different orientations of the AFM scan direction with respect to the crystal axes.

The above results argue that the observed etching is just the inverse of epitaxial growth, etching InP layer by layer. X-ray photoemission spectroscopy (XPS) analysis of the treated samples indicates the presence of inorganic sulfides possibly being attached to Indium, and organic sulfides attached to carbonaceous materials (details are given in the Supporting Information Figure S2,S3). A possible explanation for the observed layer by layer etching could be that alkyl ammonium poly sulfides initially adsorb on the InP surface, and bond to indium or phosphorous. The bonded sulfur can bridge the In-P bond to form $InPS_4$, which dissolves in the solution; thus, the layer is removed and the reaction continues for the next layer. Maeda et al.[33] have shown the same mechanism with synchrotron radiation photoelectron spectroscopy analysis of ammonium polysulfide treated InP, where the presence of indium and phosphorus polysulfides on the surface confirms sulfur binding to both In and P. Although, higher etch rates can be obtained with higher S-concentrations and/or at higher temperatures, solutions with 1.5% S concentration at 90–100 °C have reasonable etch rates (0.25–0.5 nm/min) while maintaining the epitaxial morphology. The latter etch characteristics are appropriate for controlled etching of nanostructures and removal of layers as per device requirements, without introducing defects. In the following, we present representative demonstrator applications of this etch process for sculpting pre-fabricated nanostructures and surface passivation.

Line patterns, typically 200 nm wide, made by e-beam lithography were transferred to a SiO2 layer (mask) on (100) InP substrates. These were etched at 98 °C using a 1.5% S solution, and reveal well defined etch-profiles with a height of 125 nm (Supporting Information, Figure S4). The cross-sectional profile of the gratings can be changed from over-cut to under-cut profiles

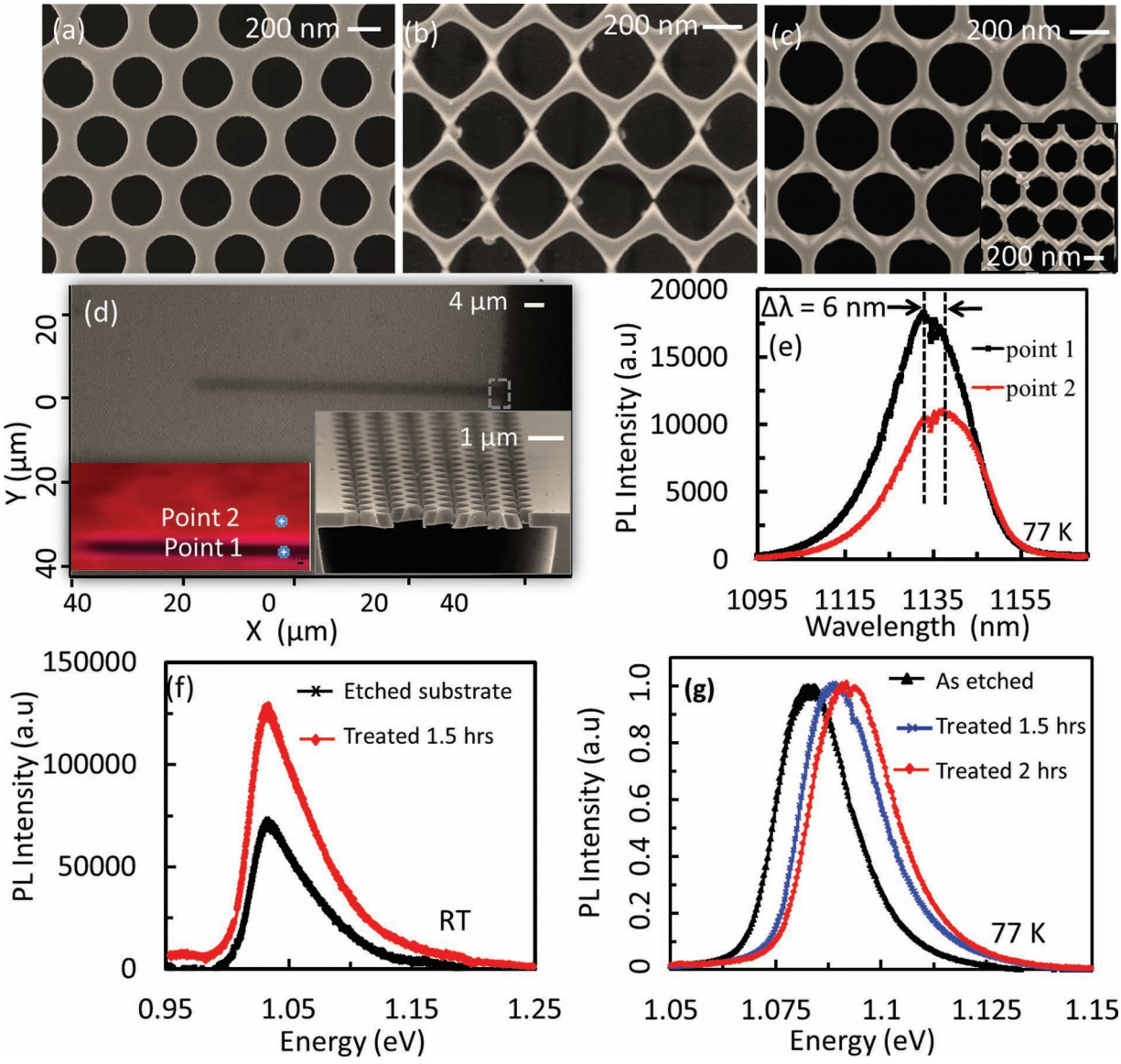

Figure 3. SEM images of representative suspended nanowires mesh samples, fabricated by reshaping circular air holes in InGaAsP membrane: a) as-fabricated structure showing the circular holes; period 420 nm and diameter 300 nm and b,c) top-views of reshaped nanowire meshes after treatment with 1.5% S solution for 1.5 h at 92 °C. The orientation of the patterns shown in (b,c) are orthogonal, and perpendicular to the {110} cleavage planes. The inset in (c) shows that the same pattern after 2 h treatment. d) Optical microscope image showing the region of the sample used for PL measurements. The corresponding spatial PL map and the SEM cross-section of the nanowire mesh are included as insets. e) PL spectra at points 1 and 2 indicated on the inset in (d). f) Comparison of PL from the InGaAsP (bulk) layer, outside the membrane, before and after treatment using 1.5% S solution for 1.5 h at 92 °C. g) Normalized PL spectra at 77 K of the suspended InGaAsP nanowire mesh for different treatment (etching) durations.

by appropriately orienting the pattern with respect to the crystal axes. The smooth surface morphology along different crystallographic planes can be used for fabrication of high quality gratings for distributed feedback (DFB) lasers. To investigate the crystallographic orientation dependence on the etch process, circular holes were fabricated in (100) InP substrates using electron beam lithography and dry etching. The rhombus shape of the hole after etching with the S—OA solution reveals the {110} etch planes (Supporting Information Figure S4). The etch rate in the [100] direction is 1.5 times faster compared to [110] with experimentally measured values of 0.42 nm/min and 0.27 nm/min, respectively. This anisotropic etching together with the highly controlled etch-rates, can be used to modify the shape of fabricated nanostructures. One example, discussed below, is that of a thin perforated membrane (here, GaInAsP).

The fabricated membranes with nanoholes having different spacings and diameters were treated with 1.5% sulfur solution (at 98 °C for 2 h), and subsequently rinsed thoroughly with isopropanol. For these experiments, we have chosen a triangular lattice of holes etched into GaInAsP/InP (**Figure 3**a). Other starting patterns are also possible, but are not investigated here. Using the anisotropic property of etching, the (dielectric)

InGaAsP veins can be made thinner while being connected in a two-dimensional network or under appropriate conditions can form disconnected single zig-zag or wavy nanowires. Different structures with very smooth surface morphologies were realized. Representative structures are shown in Figure 3b,c. The obtained shapes are consistent with anisotropic etching along the different crystal planes. Notably, the lateral dimensions could be reduced significantly, and GaInAsP veins as thin as 30 nm were obtained. In the vertical direction, the veins are still about 200 nm thick (originally 250 nm). With prolonged etching of the structures, such as those shown in Figure 3b, the sharp or pointy areas of contact can disappear altogether and entire zig-zag wires can be obtained. Preliminary experiments indeed show that generation of such free wires (appreciably long, ≈80 μm) is possible (Supporting Information Figure S5). Similarly, other geometries of long nanowires are also in principle achievable. Using a starting pattern of 1D slots in the membrane, straight nanowires with lateral dimensions ≈20 nm were obtained (Supporting Information Figure S6). Both approaches can be applied to fabricate in-plane single wire devices.

PL measurements were performed using a μ-PL set-up. An Ar laser (514 nm) was used as the excitation source, and the typical excitation spot size was ≈2 μm. The PL spectra measured from the structures (Figure 3b,c) show a small, a few nanometers, blue shift compared to the same pattern (untreated) on InGaAsP membrane or to the unpatterned portion of the membrane. The observed blue shift is attributed to lateral size reduction of the GaInAsP veins. Such a blue shift was also seen by PL mapping of the sample and the results are shown on Figure 3d,e. In addition to the wavelength shift, the data of Figure 3e shows a clear PL enhancement, despite the reduction of GaInAsP layer thickness from 250 to 200 nm. Similar PL enhancement (Figure 3f) is observed for the (bulk) GaInAsP layer in unpatterned region, sufficiently far away from the membrane. The above observations support simultaneous passivation of the GaInAsP surfaces. The PL spectra of a given patterned membrane structure, measured after different intervals of etching time show systematic shifts towards higher energies as the lateral dimensions reduce with etch time (Figure 3g). Since vertical dimension of the wire is ≈200 nm, large blue shifts in PL peak position are not expected. Thus, in a controllable manner fabricated nanostructures can be modified in size and shape, and simultaneous surface passivation is viable. Although, the results presented above are for GaInAsP, the methods are also valid for other III–V material combinations for which membranes in a chosen material can be made by suitable selective etching.

Nanopillars fabricated by colloidal lithography and inductively coupled plasma reactive ion etching (ICP-RIE),[34,35] after treatment in S—OA solution reveal very smooth surfaces. The treatment conditions can be chosen to passivate the nanopillars surface with controlled reduction of their size or with minimal change in their geometrical parameters. **Figure 4**a,b show a comparison of ICP-RIE etched InP nanopillar arrays before and after S—OA treatment, clearly demonstrating lateral size reduction without alteration of their heights. Being spherical, the colloidal silica (mask) particle has a small contact area at the top surface of the pillar. Under this area, etching in the vertical direction is prevented. However, the lateral etching reduces the diameter in a very controlled manner. In Figure 4b, it can be seen that the remnant colloidal mask particles become prominent as the nanopillars become thinner. The silica particle shows no measurable change in the silica particle size/shape, which indicates that SiO_2 is a highly selective etch-mask. The observed variation in the nanowire diameters is due to size the distribution of the colloidal silica mask particles, and is responsible for the broadening of the PL spectra for the size reduced InP and InGaAsP/InP QW nanowires. Notably, as shown in Figure 4c, nanopillars with diameters as narrow as 20 nm can be obtained (see also, Supporting Information Figure S7,S8). Since the pillar heights are ≈1 μm, this corresponds to an aspect ratio of ≈50 that is indeed remarkable for any top-down fabricated III–V nanostructure. Here, we stress that nanopillars treated with only oleylamine under the same temperature ranges and durations show neither measurable etching nor enhancement in PL. However, in striking contrast the nanopillars treated with the S—OA solution show a clear size reduction (Supporting Information Figure S9). These observations, once again confirm that the etching is due to the reaction products of S and OA, and not due to OA or impurities in it.

Normalized PL spectra (at 77 K) for the as-grown reference, as-etched, and size-reduced InP and InGaAsP/InP QW nanowires arrays are shown in Figure 4c,d, respectively. As expected, for the as-etched InP nanopillars array no PL shifts were observed since their diameters are appreciably large (> 100 nm). As for the QW pillar arrays (Figure 4d), the PL spectra are rather broad compared to the reference sample. Moreover, similar broadening of the PL spectra was observed for the as-etched QW nanopillars, which is attributed to variation in QW thickness and/or its composition.[34] Both InP (Figure 4c) and InGaAsP/InP QW (Figure 4d) size reduced nanopillars show broadened PL spectra with modest shifts of 18 and 15 meV in the peak positions, respectively, towards higher energies due to size reduction. In both cases, the lateral size variation of the wires from 20–50 nm contributes to the broadening of the respective PL peaks. Additional contribution to the broadening from composition/thickness variations in the QW pillars may be expected. Good optical properties of these wires are supported by the HRTEM data shown on Figure 4e,f for the size reduced InP and GaInAsP/InP QW pillars, respectively. The images show that high crystalline quality is maintained in the nanowires with a thin (≈2 nm) amorphous surface layer. Following the XPS analysis of blank samples treated under similar conditions (Supporting Information, Figure S2,S3), it is reasonable to assume that sulphides formed by the reaction are present on the surface.

Results discussed earlier show that simultaneous passivation is possible with S—OA solution (Figure 3e,f). Here, a similar procedure was applied, but, with negligible etching to passivate GaAs and InP. As seen in **Figure 5**a, nominally undoped epitaxial GaAs treated with S—OA solution shows a dramatic increase in PL intensity, 12 times higher, after treatment. However, with undoped epitaxial InP showed only modest increase in PL intensity was obtained. As for InP epilayers, lower surface recombination velocities could be the reason for the lower enhancement compared to GaAs. The etched InP nanopillar arrays (Figure 4a) have a low band-gap InGaAs layer which is a carrier sink; thus, making the PL intensity less sensitive to the

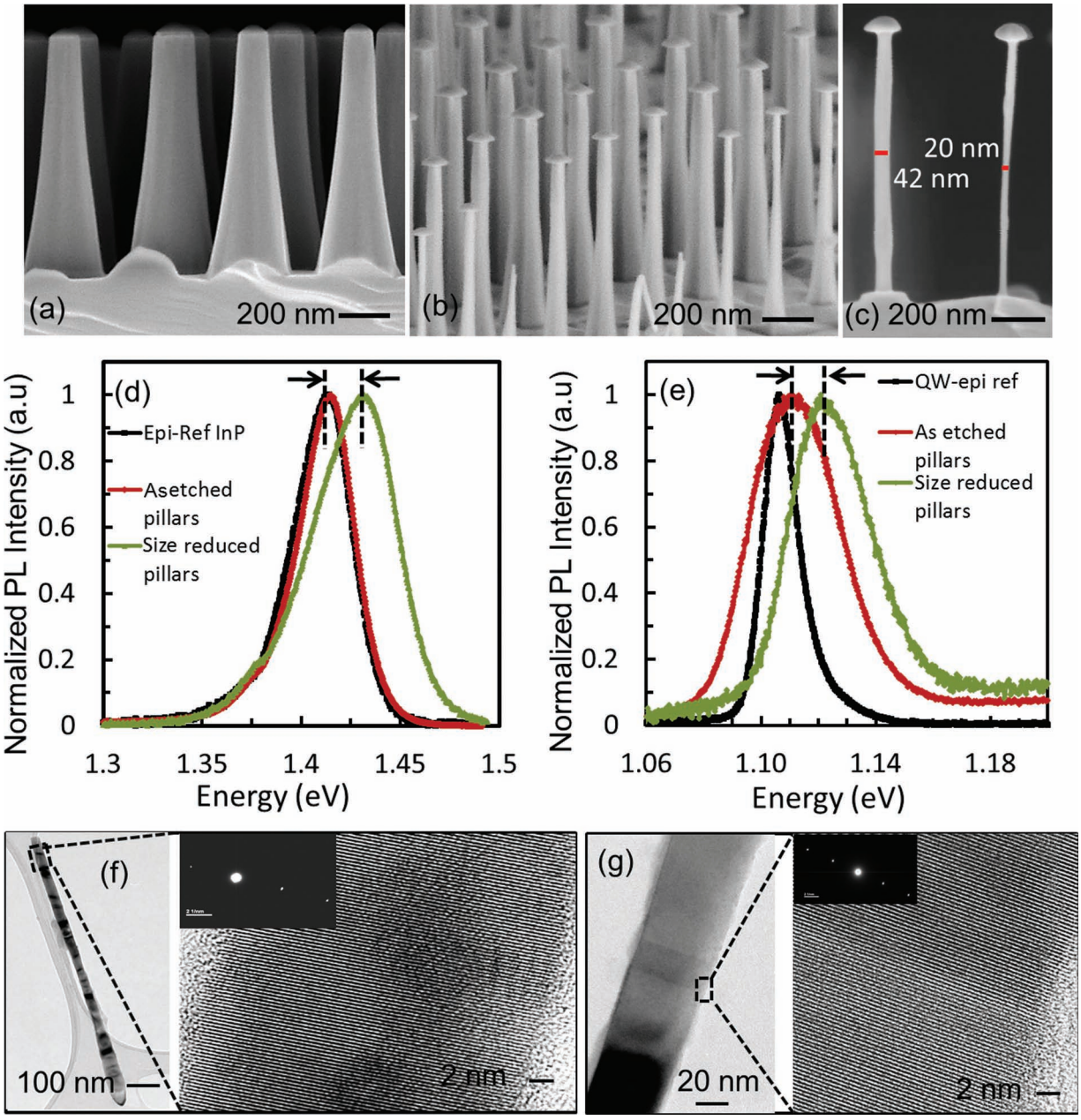

Figure 4. SEM images of InP nanopillar arrays fabricated by colloidal lithography and ICP-RIE etching: a) as etched and b) after size (diameter) reduction using the S—OA solution. In both cases, the silica (mask) particle is retained at the top. The fabricated InP/InGaAsP QW pillar arrays are also similar. c) Magnified view of a size reduced pillar sample showing that diameters as small as 20 nm (aspect ratio ≈ 50) is achievable. PL spectra of the as-etched, the size reduced nanowires, and the as-grown epitaxial (reference) samples: d) InP and e) InGaAsP/InP QW nanopillars. HRTEM analysis of size reduced nanowires showing lattice image and corresponding diffraction patterns for (100): f) InP and g) InGaAsP/InP at the interface region, showing smooth etching at the interface.

effect of passivation.[34] Therefore, to test the effect of passivation, nanopillar arrays using 150 nm SiO_2 particles as masks were fabricated on InP substrates by ICP-RIE using $Ar/CH_4/H_2/Cl_2$ etch chemistry.[35] The fabricated pillars are also narrower (inset of Figure 5b), ≈50 nm in diameter, and surface damage higher. This sample treated at ≈75 °C in S—OA solution for 1 h so as to have negligible etching, exhibited a significant increase in PL-yield up to 14 times (Figure 5b). This indicates the effect of surface passivation and is supported by XPS results on InP treated with S—OA solution (Supporting Information Figure S2,S3), which show a dramatic reduction in oxygen and the presence of inorganic sulphides. Thus, these experiments suggest that the S—OA solution can be used separately for passivating III–V surfaces in nano- and micro/macrodevice structures.

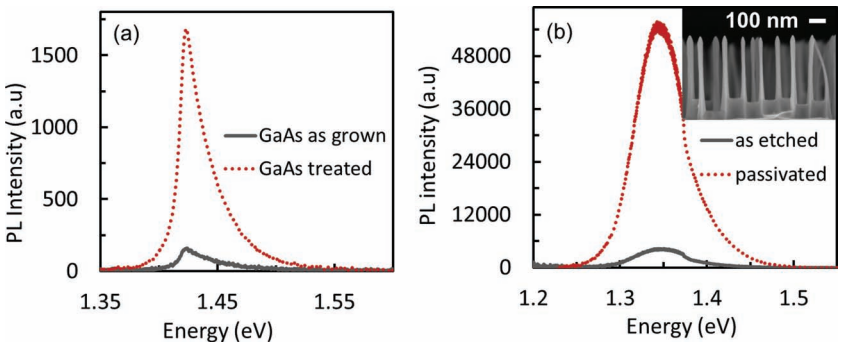

Figure 5. Passivation effect measured by PL yield from: a) GaAs epilayer before and after passivation and b) InP nanopillars before and after passivation. The inset shows a SEM image of the nanopillars.

3. Conclusions

Our results, focusing on InP-based materials, demonstrate a unique monolayer etching process based on sulfur-oleylamine solution that etches without degradation of atomic layer steps. A systematic study was conducted for controlled etching of InP and InP-based heterostructures. The results show that etching with a 1.5% S solution in a temperature range of 90–100 °C provides the optimal conditions for maintaining the step-flow morphology. The etching was found to be rate-limited and shows a clear anisotropy due to crystallographic orientation dependent etch-rates. This facile etching technique not only passivates the surfaces, but also improves the surface morphology of nano/microstructures. By applying this etch process to InP-based nano/microstructures fabricated using conventional top-down methods, high optical quality nanowires with high aspect ratios (>50) and new nanostructure geometries such as nanomesh structures and suspended (straight and zig-zag) nanowires are demonstrated. The findings are potentially interesting for III–V nanostructures and associated devices, fine tuning of resonant optical structures, generation of new nanostructure topologies, and for gate recess etching of electronic devices such as HEMTs. Although, the major focus is on InP-based materials, the results are applicable to other III–V materials such as GaAs, InAs, InSb and GaP, and associated device technologies.

4. Experimental Section

Etchant Preparation, Materials, and Etching conditions: Micropatterns generated by photolithography were transferred into a SiO_2 film on InP and used to measure the etch-depths. The etch-depth measurements were performed using a Dimension 3000 AFM with the unetched surface (obtained after removing the protecting mask) as the reference. The etch solution was prepared by dissolving sulfur in commercially available OA (technical grade, ≥70% (GC) from Sigma Aldrich). Solutions with different concentrations were prepared by dissolving 0.05, 0.5, 0.15, 0.3, 0.5 and 1.0 g of sulfur in 10 mL of oleylamine to get.05%, 0.5%, 1.5%, 3%, 5% and 10% sulfur solution in oleylamine (S—OA), respectively. Typical dissolution time of ≈1–3% sulfur in oleylamine at 70–75 °C was 1 h. The sulfur concentration in the S—OA solution was varied from 0.05% to 10% while the process temperature and duration were fixed at 92 °C and 2 h, respectively. To study effect of etch time, the samples were treated at 98 °C with a 1.5% S solution for varying durations, from 7 to 300 min. The temperature dependence of etch rate was investigated in the range from 50 to 125 °C using with a 1.5% S solution and for a fixed duration of 2 h at each temperature. To study the evolution of the etched surface morphology of epitaxial (100) InP wafers (grown by MOVPE), the samples were etched at 98 °C in a 1.5% S solution for different durations ranging from 5–135 min. Patterned samples, etched together with the epitaxial samples, were used to determine the etch-depth. Comparison of etching of other binary III–Vs such as GaAs, InSb, InAs and GaP was also investigated at 94 °C for 2 h using a 1.5% S solution.

Fabrication of Suspended Nanomesh Structures: The basic InP-based epitaxial structures were grown by MOVPE. Line-patterns (1D gratings) and hole-patterns were generated by electron-beam (e-beam) lithography. The suspended GaInAsP nanomesh structures were made from epitaxially grown InP(10 nm)/GaInAsP(250 nm) lattice matched to InP grown on InP substrate. The process steps involved deposition of 260 nm thick layer of silicon-di-oxide and e-beam lithography, followed by pattern transfer into SiO_2 layer using CHF_3 based reactive ion etching (RIE). The samples were then etched to ≈2 µm using Ar/Cl_2 chemically assisted ion beam etching (CAIBE) and subsequently treated with 50% HF for 1 min to remove the SiO_2 mask. Using 1 HCl:2 H_2O, suspended GaInAsP (patterned) membranes were then obtained by selectively removing InP beneath it. The generated air-gap below the membrane was typically >2 µm.

Nanopillar Array Fabrication: The nanopillar/wire arrays were fabricated using a combination of self-assembly of colloidal silica particles for masking and dry etching. The InP nanopillars were fabricated in a 1 µm thick epitaxially grown InP on a 300 nm InGaAs (lattice matched to InP). For the fabrication of the QW nanopillars, a 20 nm InGaAsP QW (GaInAsP lattice matched to InP; λ_{gap} = 1.22 µm) between two 200 nm thick InP barrier layers was used. The fabrication steps involved spin coating of the samples with 500 nm diameter (colloidal lithography) SiO_2 particles, size reduction of the particles by plasma etching, and finally dry etching using ICP-RIE with $CH_4/H_2/Cl_2$ chemistry.[34] Depending on the required size, the pillars were etched for different durations ranging from 60–110 min at 92 °C using 1.5% S solution. After treatment, the samples were rinsed in isopropanol and blow-dried using nitrogen.

Characterization Methods: Surface morphology and etch-depth measurements were performed by a Dim 3000 atomic force microscope operated in tapping mode using commercial Si probes from Nanosensors GmBH. The geometrical parameters of the fabricated nanostructures, including side-wall surface morphology, were determined by high resolution scanning electron microscopy (SEM). µ-photoluminescence (PL) measurements including mapping PL were performed using a Lab-RAM system from HORIBA Jobin-Yvon. Argon laser with excitation wavelength of 514 nm and a spot size of about 2 µm was used. Transmission electron microscopy (TEM) analysis was performed using a JEM-2001 (JOEL) field emission transmission electron microscope working at 200 keV. The size reduced InP nanowires were released from substrate by selectively etching the InGaAs sacrificial layer whereas the QW nanowires were gently scratched from InP substrate. The wires were suspended in isopropanol and dispersed on copper grids for TEM analysis.

Supporting Information

Supporting Information is available from the Wiley Online Library or from the author.

Acknowledgements

The work was performed within the Linné Center for Advanced Optics and Photonics (ADOPT). The work was supported by the Swedish

Research Council (Grant number: 349-2007-8664), the EU-FP7 project Nanophotonics for Energy Efficiency (Grant number: 248855) and the Nordic Innovation Center project Nanordsun (Grant number: 10048). S.N. and N.S. acknowledge the Higher Education Commission of Pakistan for partially supporting their PhD studies. The authors thank M. Hammar and J. Berggren for MOVPE growth and A. Berrier and G. Landgren for useful discussions.

Received: August 3, 2012
Published online: October 26, 2012

[1] X. Duan, Y. Huang, Y. Cui, J. Wang, C. M. Lieber, *Nature* **2001**, *409*, 66.
[2] S. L. Diedenhofen, G. Vecchi, R. E. Algra, A. Hartsuiker, O. L.Muskens, G Immink, E. P. A. M. Bakkers, W. L Vos, J. G. Rivas, *Adv. Mater.* **2009**, *21*, 973.
[3] M. T. Björk, B. J. Ohlsson, T. Sass, A. I. Persson, C. Thelander, M. H. Magnusson, K. Deppert, L. R. Wallenberg, L. Samuelson, *Nano Lett.* **2002**, *2*, 87.
[4] H. Kind, H. Yan, B. Messer, M. Law, P. Yang, *Adv. Mater.* **2002**, *14*, 158.
[5] K. Haraguchi, T. Katsuyama, K. Hiruma, *J. Appl. Phys.* **1994**, *75*, 4220.
[6] A. I. Hochbaum, R. Chen, R. D. Delgado, W. Liang, E. C. Garnett, M. Najarian, A. Majumdar, P. Yang, *Nature* **2008**, *451*, 163.
[7] Y. Cui, Q. Wei, H. Park, C. M. Lieber, *Science* **2001**, *293*, 1289.
[8] Q. Qing, S. K. Pal, B. Tian, X. Duan, B. P. Timko, T. Cohen-Karni, V. N. Murthy, C. M. Lieber, *Proc. Natl. Acad. Sci. USA* **2010**, *107*, 1882.
[9] R. Chau, B. Doyle, S. Datta, J. Kavalieros, K. Zhang, *Nat. Mater.* **2007**, *6*, 810.
[10] T. Enoki, H. Ito, K. Ikuta, Y. Umeda, Y. Ishii, *Microwave Opt. Technol. Lett.* **1996**, *11*, 135.
[11] T. Bryllert, L.-E. Wernersson, L. E. Froberg, L. Samuelson, *IEEE Electron. Device Lett.* **2006**, *27*, 323.
[12] J. Faist, F. Capasso, D. L. Sivco, C. Sirtori, L. A. Hutchinson, A. Y. Cho, *Science* **1994**, *264*, 553.
[13] D. L. Huffaker, G. Park, Z. Zou, O. B. Shchekin, D. G. Deppe, *Appl. Phys. Lett.* **1998**, *73*, 2564.
[14] L. K. van Vugt, S. J. Veen, E. P. A. M. Bakkers, A. L. Roest, D. Vanmaekelbergh, *J. Am. Chem. Soc.* **2005**, *127*, 12357.
[15] Q. Hang, F. Wang, P. D. Carpenter, D. Zemlyanov, D. Zakharov, E. A. Stach, W. E. Buhro, D. B. Janes, *Nano Lett.* **2008**, *8*, 49.
[16] Y. Akahane, T. Asano, B.-S. Song, S. Noda, *Nature* **2003**, *425*, 944.
[17] K. Hennessy, A. Badolato, A. Tamboli, P. M. Petroff, E. Hu, M. Atatüre, J. Dreiser, A. Imamoğlu, *Appl. Phys. Lett.* **2005**. *87*, 021108.
[18] Y. Sun, D.-Y. Khang, K. Hurley, R. G. Nuzzo, J. A. Rogers, *Adv. Funct. Mater.* **2005**, *15*, 30.
[19] T. Meguro, M. Hamagaki, S. Modaressi, T. Hara, Y. Aoyagi, M. Ishii, Y. Yamamoto, *Appl. Phys. Lett.* **1990**, *56*, 1552.
[20] G. C. DeSalvo, C. A. Bozada, J. L. Ebel, D. C. Look, J. P. Barrette, C. L. A. Cerny, R. W. Dettmer, J. K. Gillespie, C. K. Havasy, T. J. Jenkins, K. Nakano, C. I. Pettiford, T. K. Quach, J. S. Sewell, G. D. Via, *J. Electrochem. Soc.* **1996**, *143*, 3652.
[21] H. E. Hessel, A. Feltz, M. Reiter, U. Memmert, R. J. Behm, *Chem. Phys. Lett.* **1991**, *186*, 275.
[22] X. Cao, I. Thayne, *Microelectron. Eng.* **2003**, *67–68*, 333.
[23] K. Hayashi, S. Yamanaka, H. Okushi, K. Kajimura, *Diamond Relat. Mater.* **1996**, *5*, 1002.
[24] S. D. Park, C. K. Oh, J. W. Bae, G. Y. Yeom, T. W. Kim, J. I. Song, J. H. Jang, *Appl. Phys. Lett.* **2006**, *89*, 043109.
[25] J. C. Love, L. A. Estroff, J. K. Kriebel, R. G. Nuzzo, G. M. Whitesides, *Chem. Rev.* **2005**, *105*, 1103.
[26] V. N. Bessolov, M. V. Lebedev, *Semiconductors* **1998**, *32*, 1141.
[27] H. Lim, C. Carraro, R. Maboudian, *Langmuir* **2004**, *20*, 743.
[28] Y. Gu, Z. Lin, R. A. Butera, V. S. Smentkowski, D. H. Waldeck, *Langmuir* **1995**, *11*, 1849.
[29] M. Schvartzman, V. Sidorov, D. Ritter, Y. Paz, *J. Vac. Sci. Technol., B.* **2003**, *21*, 148.
[30] Y. Jun, X.-Y. Zhu, J. W. P. Hsu, *Langmuir* **2006**, *22*, 3627.
[31] M. T. Sheldon, C. N. Eisler, H. A. Atwater, *Adv. Energy Mater.* **2012**, *2*, 339.
[32] M. H. Sun, H. J. Joyce, Q. Gao, H. H. Tan, C. Jagadish, C. Z. Ning, *Nano Lett.* **2012**, *12*, 5325.
[33] F. Maeda, Y. Watanabe, M. Oshima, *Appl. Phys. Lett.* **1993**, *62*, 297.
[34] S. Naureen, R. Sanatinia, N. Shahid, S. Anand, *Nano Lett.* **2011**, *11*, 4805.
[35] M.-Y. Li, S. Naureen, N. Shahid, S. Anand, *J. Electrochem. Soc.* **2010**, *157*, 896.